X-ray spectra and electronic structure of Sc and Ti dihydrides



2008 J. Phys.: Condens. Matter 20 335224

(http://iopscience.iop.org/0953-8984/20/33/335224)

J. Phys.: Condens. Matter **20** (2008) 335224 (6pp) doi:10.1088/0953-8984/20/33/335224

# X-ray spectra and electronic structure of Sc and Ti dihydrides

**A V Galakhov[1], L D Finkelstein[1], E Z Kurmaev[1], R G Wilks[2], A Moewes[2] and V K Fedotov[3]**

[1] Institute of Metal Physics, Russian Academy of Sciences—Ural Division, 620041 Yekaterinburg GSP-170, Russia
[2] Department of Physics and Engineering Physics, University of Saskatchewan, Saskatoon, SK, 57N 5E2, Canada
[3] Institute of Solid State Physics, Russian Academy of Sciences, Chernogolovka, Moscow District 142432, Russia

Received 20 March 2008, in final form 6 July 2008
Published 31 July 2008
Online at stacks.iop.org/JPhysCM/20/335224

**Abstract**

We measured x-ray resonant and nonresonant emission and absorption spectra of $Sc_2O_3$ and emission spectra of $ScH_2$, $ScD_2$ and $TiH_2$. *Ab initio* generalized gradient approximation calculations of the electronic structure are performed using the experimental crystal structures as input. The dependence of the resonant x-ray spectra on the excitation energy is measured and the difference between that for $Sc_2O_3$ and that for $ScH_2$ and between that for $ScH_2$ and that for $TiH_2$ is shown. The difference is due to the dominance of ionization over excitation processes in hydrides and higher 3d filling in Ti with respect to Sc. Good agreement between calculated and experimental spectra is found.

## 1. Introduction

Sustained investigations of dilute solid hydrogen solutions and hydrides of rare-earth metals [1–3], as well as a recent study of Re–H solid solutions [4] have yielded unexpected results concerning the environments of the hydrogen atoms in these substances. When the local symmetries of the hydrogen atoms are examined using NMR, inelastic neutron scattering (INS), or optical and IR spectroscopy, they are always lower than the symmetry that is predicted by the results of neutron diffraction studies. A comparative analysis of the INS and neutron diffraction data for trihydrides of scandium [5] and yttrium [6] showed that the neutron diffraction gives the average long-range symmetry of the structure, and that the hydrogen sublattices have additional short-range ordering. It is this short-range displacive ordering that results in the lowering of the local symmetry of the hydrogens, which affects the properties measured by spectroscopic techniques.

An electron diffraction examination of scandium dihydride reveals small domains (5–10 nm across) with cubic $Mn_2O_3$-type superstructure [7]. It had previously been believed that $ScH_2$ has a more symmetrical $CaF_2$-type structure with the hydrogen atoms occupying tetrahedral interstitial sites in the fcc metal lattice. The $Mn_2O_3$-type structure of $ScH_2$ can be formed from the $CaF_2$-type structure by correlated displacements of Sc and H atoms from their symmetrical positions, with the new positions of the Sc atoms corresponding to two crystallographically inequivalent sites. Resonant and nonresonant x-ray emission spectra (RXES, NXES) provides direct information about the local partial density of electronic states, and were used to determine whether there are any experimentally detectable differences between the inequivalent Sc sites. The x-ray scattering spectra of $ScH_2$ and $ScD_2$ were compared to those of $Sc_2O_3$, which has $Mn_2O_3$-type structure, and $TiH_2$, which has $CaF_2$-type structure. We also carried out *ab initio* electronic structure calculations using the same method for all compounds. The comparison of these calculations to the measured spectra allows us to determine significant electronic properties of the compounds, such as the filling of the bands. The electronic structure of these compounds was previously calculated in [8, 9]; however, no previous calculations of x-ray spectra are available.

## 2. The structural data

The samples have been prepared using the method described in [5, 7]. According to the x-ray and neutron scattering measurements [7], $ScH_{1.89}$ and $ScD_{1.99}$ at room temperature have $CaF_2$-type structure with cubic lattice parameters of $a_0 = 4.7833$ and 4.7706 Å respectively. In spite of the

 

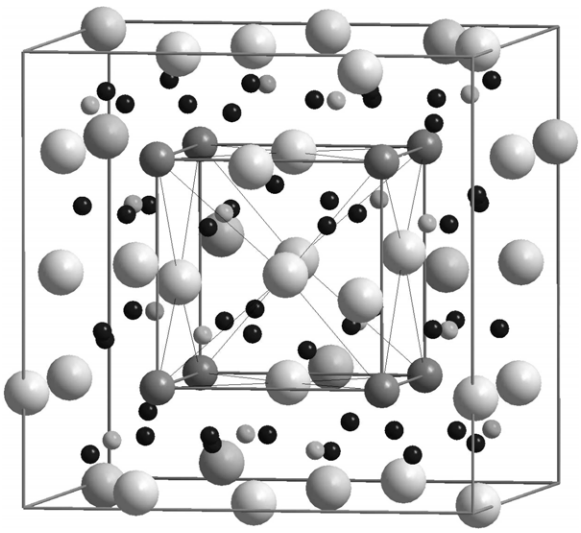

**Figure 1.** Crystal structure of $ScH_2$. The larger spheres represent Sc sites and the smaller spheres represent hydrogen sites. The inequivalent Sc and H sites are denoted by the differences in tints and radii of spheres.

vibrational symmetry, the local environment of the hydrogen atoms in these dihydrides is not cubic. It is likely that this disagreement is a reflection of the fact that traditional (integral) diffraction methods provide a measurement of the averaged lattice parameters, whereas the local order structure that determines the hydrogen potential may be more complicated. Transmission electron diffraction measurements suggest that the positions of the hydrogen atoms can be described as a superstructure that is the result of deformation of the fcc lattice. This superstructure is simulated as a cubic cell with double parameter $A = 2a_0$ and bcc-type (1/2, 1/2, 1/2) translation. We assume that the $ScH_{1.89}$ and $ScD_{1.99}$ structures are close to that of $ScH_2$ ($Mn_2O_3$-type, space group $Ia3$ (No. 206), and positions [48e $(x, y, z)$ 24d $(x, 0, 1/4)$ 16c $(x, x, x)$ 8b (1/4, 1/4, 1/4) 8a(0, 0, 0)]). For $Sc_2O_3$, $A = 9.841$ Å and the atom positions are (Sc1) 8b (0.2500, 0.2500, 0.2500), (Sc2) 24d (0.9645, 0.0000, 0.2500), and (O) 48e (0.3914, 0.1548, 0.3814). Because the Sc2 and hydrogen positions for $ScH_{1.89}$ could not be determined by electron diffraction, they are assumed to be similar to the corresponding positions in the oxide.

There are similarities between the crystal structures of $Sc_2O_3$ and $ScH_2$: the fcc cell of the metal forms the basis of both structures, which causes the ions to be divided into two types and to have $Cu_3Au$-type ordering. Atomic shifts and tetrapore distortion also occur as a result of the lowering of the hydrogen point symmetry from cubic to hexagonal that occurs as a result of this division of the ions. The superstructures of the dihydrides are somewhat different from those of the oxides because of the lower cell parameter (by about 3%), the smaller shift of atoms, and smaller tetrapore distortion. This last difference leads to occupation of tetrahedrons of the second type (H2) by an additional hydrogen in the 16*c* position, resulting in the integral composition of $ScH_2$. In the oxide, these tetrapores are blocked, leading to the $Sc_2O_3$ formula.

**Table 1.** Atom coordinates of fluorite-like scandium compounds.

| Atom | Pos. | $x$ | $y$ | $z$ |
|---|---|---|---|---|
| Sc1 | 8b | 0.2500 | 0.2500 | 0.2500 |
| | | 1/4 | 1/4 | 1/4 |
| Sc2 | 24d | 0.9645 | 0.0000 | 0.2500 |
| | | $\mathbf{1} - 0.0355$ | 0 | 1/4 |
| O1 (H1) | 48e | 0.3914 | 0.1548 | 0.3814 |
| | | $\mathbf{3/8} + 0.0164$ | $\mathbf{1/8} + 0.0298$ | $\mathbf{3/8} + 0.0064$ |

The structure of $Sc_2H_3H$ is of $Sc_2O_3$ type, consisting of 16 formula units per unit cell with $A = 2a_0$, is shown in figure 1. The $Cu_3Au$-type fcc structure with $a_0$ $(Sc^1)_3$ $(Sc^2)$ is described by the lines within the cell. In the small distorted fluorite-type part, H1 and H2 occupy quasitetrahedral positions with a small shift that corresponds to 24e and 16c of the large cell (space group $Ia3$, $A = 2a_0$). The value of these shifts can be determined with respect to ideal positions in the fluorite cell. These shifts, estimated for the oxide, are shown in table 1.

For the Sc dihydride, the shifts should have smaller values, leading to the filling of the additional position 16c $(x, x, x)$, near $x = \mathbf{3/8}$. In this model, $ScH_2$ and $ScD_2$ have exactly the same structure.

If the nonequivalent Sc1 (8b) and Sc2 (24d) sites in $Sc_2O_3$ can be detected experimentally using x-ray scattering, then these observations can be used to deduce structural information about the scandium dihydrides. If nonequivalent Sc atoms can be detected in the Sc oxide, then they will also be found in the hydride, regardless of the isotope type.

## 3. Experimental and calculational details

X-ray absorption and emission spectra were measured at Sc and Ti L-edges at room temperature at beamline 8.0.1 of the Advanced Light Source at Lawrence Berkeley National Laboratory. The $L_{2,3}$ emission spectra reflect mainly 3d $\rightarrow$ $2p_{3/2}$ ($L_3$) and 3d $\rightarrow$ $2p_{1/2}$ ($L_2$) dipole transitions. Spectra were recorded for dihydrides $TiH_2$, $ScH_{1.89}$ and $ScD_{1.99}$ as well as for the reference sample $Sc_2O_3$. The absorption spectra were measured in total electron yield (TEY) mode, and all spectra were normalized to the intensity of the incoming beam.

We calculated the total and partial densities of states and the metal x-ray emission spectra for $TiH_2$, $ScH_2$ and $Sc_2O_3$. For $Sc_2O_3$ the XAS spectrum was also simulated. Some other information from the calculations, including the dispersion and occupation numbers, were also analyzed. The *ab initio* electronic structure calculations were performed using a one-electron model. The Wien2k computation package [10] was used. All of the calculations used the GGA method [11, 12], and took only our structural data as input. Muffin-tin radii $R_{MT}$ used in calculations are 1.500 au for hydrogen and 2.000 au for Sc and Ti in $ScH_2$ and $TiH_2$. In $Sc_2O_3$ we used $R_{MT} = 2.0700$ au for Sc and 1.8300 au for the oxygen. The parameter $RK_{max}$ was 7.00 for all calculations. Here $K_{max}$ is the maximum reciprocal lattice vector to be taken into account and $R$ is the minimum muffin-tin radius. As the experimental measurements of the crystal structure are accurate enough, no structural optimization was necessary. The convergence was

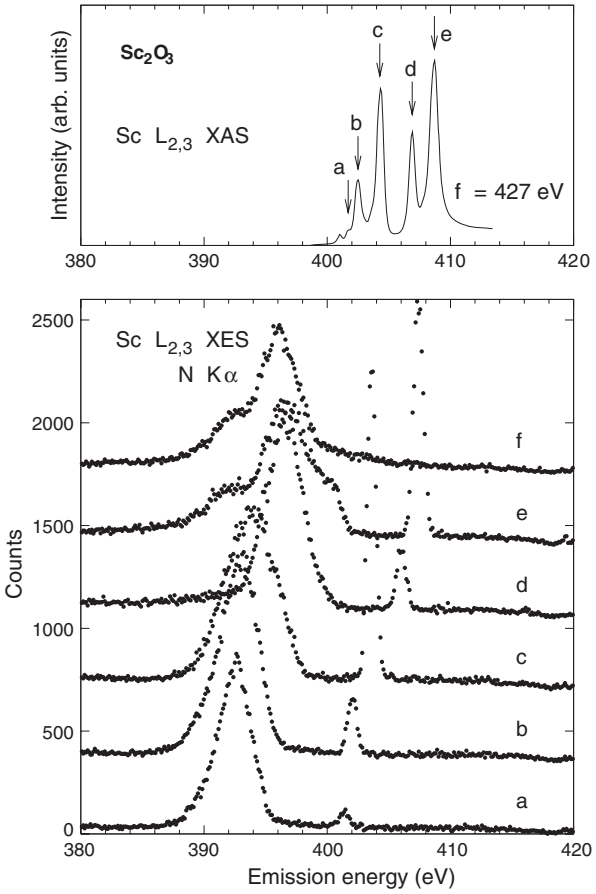


**Figure 2.** X-ray Sc $L_{2,3}$ absorption spectra and resonant ('a'–'e') and nonresonant ('f') $L_{2,3}$ emission spectra of $Sc_2O_3$.

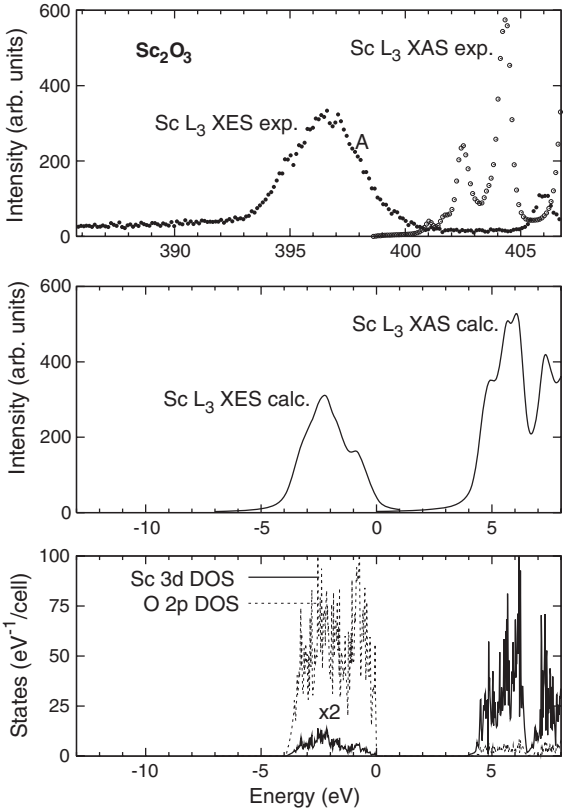


**Figure 3.** Experimental and calculated x-ray emission spectra of $Sc_2O_3$ compared to its DOS. The DOS below 0 eV is multiplied by 2.

good with the total energy error less than $10^{-5}$ Ryd. Our results are in good agreement to the ones from [8, 9]. To facilitate comparison with the measured XES and XAS spectra, well-known lifetime broadening parameters ($\gamma_0$ was 0.4 eV for Sc and 0.7 eV for Ti for the core states, $W = 0.1$ eV for the valence states of both Sc and Ti) were the only non-structural input to the calculations.

## 4. Results and discussion

Figure 2 shows the Sc 2p x-ray absorption spectra and resonant ('a'–'e') and nonresonant ('f') Sc $L_3$ emission spectra of $Sc_2O_3$. Some ammonia compounds were used in the synthesis of $Sc_2O_3$. As a result, the N K$\alpha$ line (corresponding to the $2p \rightarrow 1s$ transition) appears at 392.4 eV in the emission spectra when the excitation energy is greater than the nitrogen 1s excitation energy. The N line forms a clearly separable feature for excitation energies 'f' and 'e.'

A major feature of the emission spectra is the existence of high-intensity peaks of elastically scattered radiation, which are most prominent when the excitation energy is set to the main peaks in the Sc 2p XAS spectrum. The appearance of these strong elastic peaks indicates that the probability of exciting the Sc 2p core electron to a bound state is high with respect to the ionization process. The appearance of the main Sc $L_3$ emission line is strongly affected when the excitation energy is varied. This clearly shows its RXES nature, which arises from d–d energy loss transitions which occur approximately 8.0 eV below the elastic peaks. According to figure 3, this transition corresponds to the excitation of Sc d electrons from the occupied states into vacant states.

Figure 2 shows that when $E_{exc}$ is within the Sc $L_3$ energy range, most of the inelastic line's intensity is located in the $L_3$ RXES. In contrast, when $E_{exc}$ is in the Sc $L_2$ energy range the nonresonant (NXES) $L_3$ features become more prominent. We believe that the $L_3$ ionization threshold is located at approximately $E_{exc} = 405$ eV.

When resonantly exciting the Sc $L_2$ transitions, the elastic scattering lines are not less intense than for the Sc $L_3$ XES. The inelastic $L_2$ RXES cannot be seen, as they are found at the same energy as the Sc $L_3$ NXES. The Sc $L_2$ NXES are much smaller than Sc $L_3$ NXES, which is likely the result of the Coster–Kronig process. The Sc $L_2$ RXES are unaffected by the Coster–Kronig effect. This is probably due to the exciton bonding between the excited core level electron and the $L_2$ hole, which would tend to prevent the hole from moving to the $L_3$ level.

Figure 3 compares the experimental Sc $L_3$ NXES to the calculations of both the NXES and the Sc 3d DOS. Feature *A* of the experimental spectrum appears in the calculations, and has its origin in hybrid Sc 3d and O 2p states. The GGA calculation represents the location of the valence and

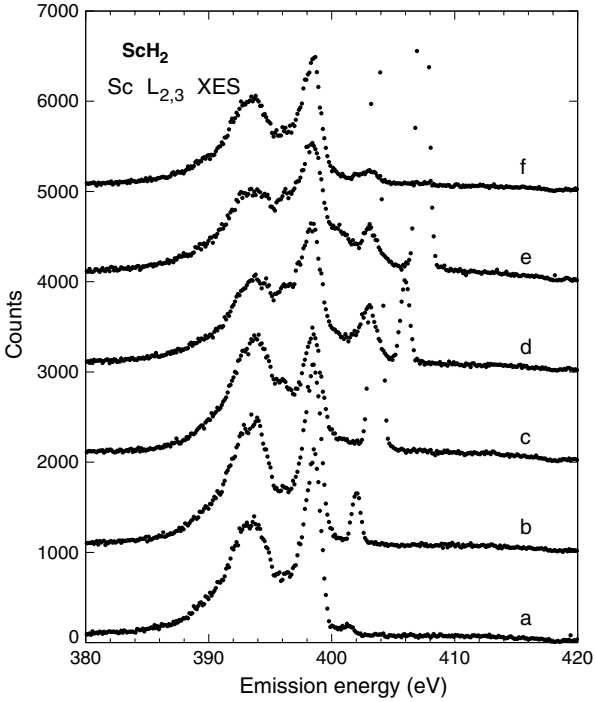


**Figure 4.** Sc $L_{2,3}$ x-ray emission spectra of $ScH_2$.

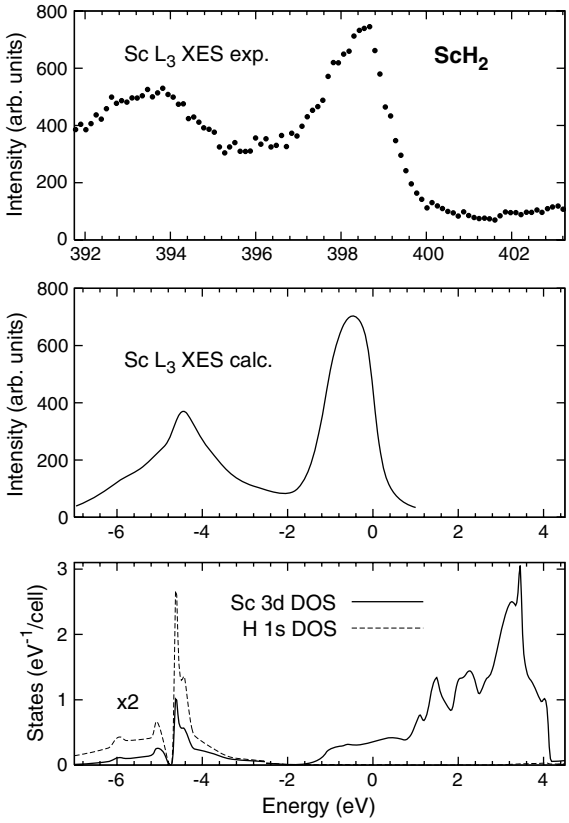


**Figure 5.** Experimental and calculated x-ray emission spectra of $ScH_2$ compared to its DOS. The lower part of DOS is multiplied by 2.

unoccupied states quite well. Densities of states of $Sc_2O_3$ show strong hybridization between Sc 3d and O 2p states across the whole valence band. The existence of the hybridization is confirmed by studying the calculated $E(\vec{k})$ dependencies (not shown here). The following ion charges were found: Sc: $+1.38$e, O: $-0.92$e.

There is some disagreement between the calculated absorption spectrum and the experimental one, which is most likely caused by the effect of the 2p hole that is present in the final state of the absorption process. Without the inclusion of the core hole in the model, local and semilocal approaches such as GGA are generally not suitable for describing such excited states.

Figure 4 shows the Sc $L_{2,3}$ XES spectra of $ScH_2$, which are indistinguishable from the corresponding spectra of $ScD_2$. The excitation energies were the same as for $Sc_2O_3$. The TEY absorption spectrum shows signs of surface oxidation, and is not included here. The bulk-sensitive emission measurements are not affected by oxidation.

The strong differences between the hydride and oxide $L_3$ emission spectra are likely due to the affinity of the ionization and excitation thresholds in the hydride. It is likely that the Sc in the hydride has a more neutral, atom-like state than in $Sc_2O_3$. The influence of the charge state of the cation on the characteristics of the ionization and excitation thresholds was studied in [13].

Figure 5 shows the comparison between the experimental and calculated Sc $L_3$ XES as well as the H 1s and Sc 3d DOS. Overall, the agreement between the measured and calculated XES is quite good, suggesting that the model used for the calculations was appropriate and can be used to analyze properties which cannot be observed experimentally. The Fermi level lies in the Sc 3d band indicating the existence of the d electron in two-valence Sc and the metallic character of this compound. The exact location of $E_F$ in the experimental spectrum depends on the stoichiometry of the sample. Because dihydrides tend to partially lose their hydrogen atoms, there tend to be more filled Sc 3d sites in a real sample than in the theoretical model; i.e. the real Fermi energy is higher than the calculated one. To show this, we performed a series of calculations for a $ScH_{2-\delta}$ model. In these calculations $E_F$ shifts to higher energies as a function of $\delta$, in good agreement with the experimental results.

In contrast to the $Sc_2O_3$, the upper part of the $ScH_2$ valence band is almost completely d-like and only in its lower part is there an overlap between the hydrogen 1s and metal 3d states. The hydrogen states are dominant in this portion of the DOS. Analysis of the results of the calculations shows that there is strong hybridization in the lower-energy portion of the DOS, originating between the $X$, $Z$, $W$ and $K$ points of the Brillouin zone. In contrast, the upper one has the same origin for the metal only. There is also a small contribution from the hydrogen that is not visible in the DOS pictures. Analysis of the electron dispersion calculations (see figure 6) shows that this hydrogen contribution originates from a small area near $\Gamma$.

This hydrogen contribution does not represent hybridization with the metal 3d states since hydrogen and metal states have different $\vec{k}$-vectors at these energies. The hybridization in $ScH_2$ is quite weak and occurs only around $-4$ eV. Also, the

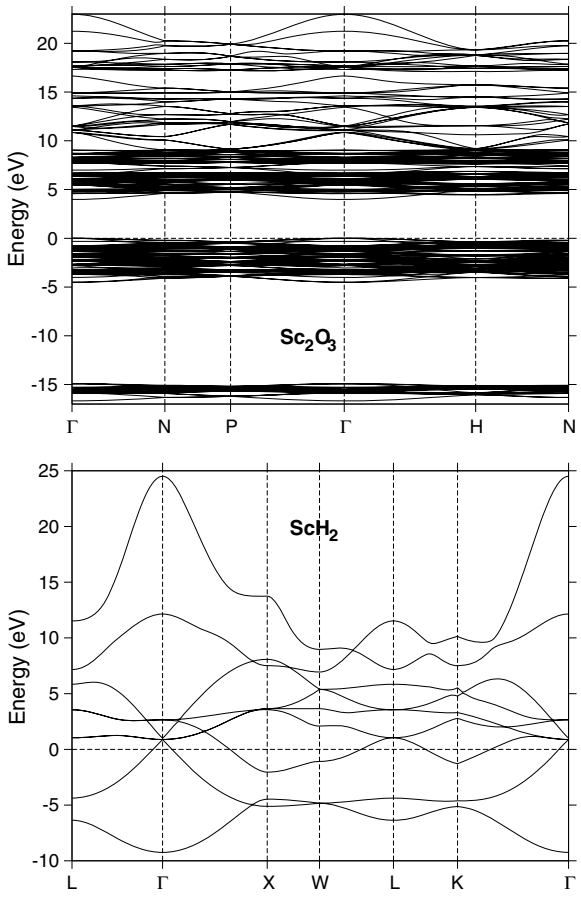


**Figure 6.** Dispersion curves of $Sc_2O_3$ and $ScH_2$.

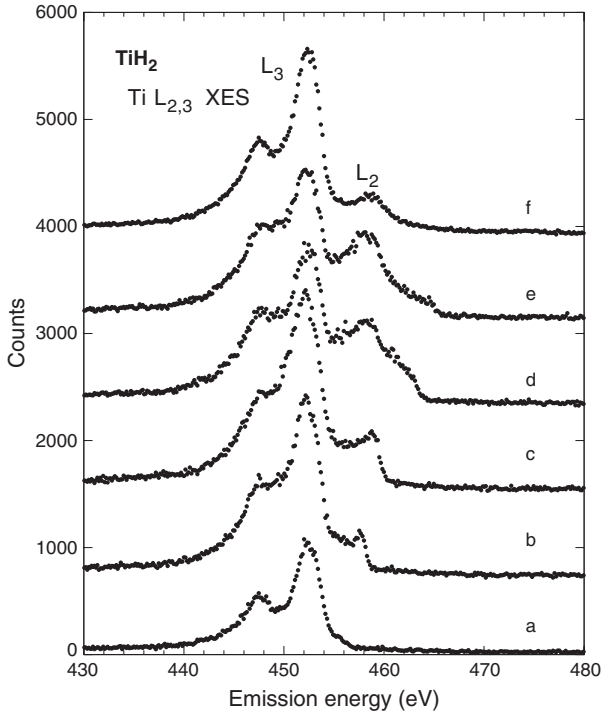


**Figure 7.** Ti $L_{2,3}$ x-ray emission spectra of $TiH_2$.

atoms remain basically uncharged (Sc: +0.025e, H: −0.05e, interstitial H: +0.075e). These results show that $ScH_2$ is not ionic but covalent and even intercalate-like, in contrast to strongly ionic $Sc_2O_3$.

The results of the measurements of $TiH_2$ are quite similar to what was seen for $ScH_2$, and the spectra are shown in figures 7, 8. Figure 7 shows the Ti $L_{2,3}$ XES. Surface oxidation was a problem for this sample, as it was for $ScH_2$, and so again the XAS is not shown. Therefore, the $E_{exc}$ values were chosen to correspond to features of the Ti $L_{2,3}$ XAS of $TiO_2$. In figure 7 the weakness of the elastic peaks of Ti $L_{2,3}$ RXES is noticeable. This can reasonably be attributed to a decrease in the $L_{2,3}$ absorption coefficients as a result of the filling of the 3d states.

In the inelastic portion of the emission spectra, the nonresonant $L_{2,3}$ XES is the dominant process, while there is little to no contribution from the $L_{2,3}$ RXES. As in $ScH_2$, the $L_{2,3}$ NXES is associated with decay from two bands: one d-like and one H 1s-like. These bands are separated by about 5 eV. The only major difference is in the relative intensities of the emission: $I_{Me\ 3d}/I_{H\ 1s}$ is about 2.0 for $ScH_2$ and as high as 3.4 for $TiH_2$. This difference is undoubtably caused by the addition of one electron to the Me 3d band when going from Sc to Ti.

Figure 8 shows the comparison of the experimental and calculated spectra and the calculated DOS of $TiH_2$. As was found with the $ScH_2$ calculations, there is good agreement between the calculated and measured XES. The change in the $I_{Me\ 3d}/I_{H\ 1s}$ ratio is reproduced in the XES calculation. The location of $E_F$ is also found to be dependent on $\delta$ in $TiH_{2-\delta}$ as with $ScH_2$. The Fermi energy in the experimental result is shifted to higher energy with respect to the calculation for stoichiometric $TiH_2$.

From the calculation, we see that $TiH_2$ behaves just like $ScH_2$. It therefore follows that the differences in the local densities of states between the hydride and the oxide arise because the oxide has Sc 3d and O 2p states hybridized within the whole valence band, while there exists within the hydride an upper part of the valence band that is not hybridized with the hydrogen. This band crosses the Fermi level into the unoccupied states. The band belongs to the metal atom and retains a strong 3d character. As the energy bands of both Me and H go through the entire Brillouin zone, both the energy overlap and the $k$-correspondence must be taken into account to distinguish between the hybridization and simple energy overlap.

## 5. Conclusions

We have performed resonant and nonresonant x-ray emission, and x-ray absorption measurement, as well as *ab initio* electronic structure calculations of $ScH_2$, $TiH_2$, and $Sc_2O_3$. There is excellent agreement between the calculated and measured nonresonant x-ray spectra, confirming that the calculations can be used to predict properties of these compounds. We found strong hybridization between Sc and O across the entire valence band in $Sc_2O_3$, in contrast to the

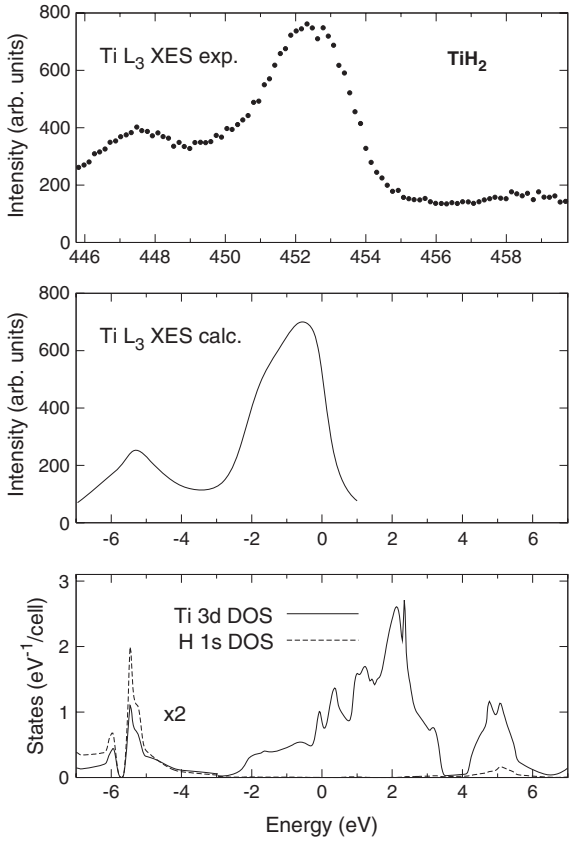


**Figure 8.** Experimental and calculated x-ray emission spectra of $TiH_2$ compared to the partial DOS. The lower part of DOS is multiplied by 2.

metal dihydrides, where almost no hybridization takes place in the upper bands.

This study uncovered some new properties of the Me $L_{2,3}$ XES of the compounds in question. First, the intensity ratio of the NXES and RXES inelastic parts is dependent on the charge state of the 3d element. The decrease in the cation charge when going from the oxide to hydride results in a shift of the intensity of the spectra from the RXES to the NXES region. This shift results from the closeness of the ionization and excitation thresholds in the hydrides. The ionization process seems to suppress the d–d transition in the excitation channel as the inelastic features in hydrides RXES do not appear while the energy distance between the vacant and occupied DOS maximums is the same. For hydrides with different d elements, an increase of the $I_{\mathrm{Me\ 3d}}/I_{\mathrm{H\ 1s}}$ ratio and a decrease in the intensity of the RXES elastic peaks was observed as a result of the filling of the 3d shell.

## Acknowledgments

This work was supported by the Russian Foundation for Basic Research (grant Nos 04-02-17269 and 08-02-00148), the Research Council of the President of Russian Federation (grant NSH-1929.2008.2), Natural Sciences and Engineering Research Council of Canada (NSERC), Integration Project of the Ural and Siberian Divisions of the Russian Academy of Sciences, and the Canada Research Chair program.

## References

[1] Vajda P 1995 *Handbook on the Physics and Chemistry of Rare Earths* vol 20 (Amsterdam: Elsevier) chapter 137, p 207
[2] Udovic T J, Rush J J, Huang Q and Anderson I S 1997 *J. Alloys Compounds* **253** 4
[3] van Gelderen P, Kelly P J and Brocks G 2003 *Phys. Rev.* B **68** 094302
[4] Antonov V E, Fedotov V K, Harkunov A I, Kolesnikov A I, Novokhatskaya N I, Grosse G, Wagner F E, Hansen T and Ivanov A S 2001 *Phys. Rev.* B **64** 184302
[5] Antonov V E, Bashkin I O, Fedotov V K, Khasanov S S, Hansen T, Ivanov A S, Kolesnikov A I and Natkaniec I 2006 *Phys. Rev.* B **73** 054107
[6] Fedotov V K, Antonov V E, Bashkin I O, Hansen T and Natkaniec I 2006 *J. Phys.: Condens. Matter* **18** 1593
[7] Antonov V E, Bashkin I O, Fedotov V K, Nikolaichik V I, Natkeniec I, Padurets L N and Shilov A L 2008 in preparation
[8] Miwa K and Fukumoto A 2002 *Phys. Rev.* B **65** 155114
[9] Koitzsch C, Hayoz J, Bovet M, Clerc F, Despont L, Ambrosch-Draxl C and Aebi P 2004 *Phys. Rev.* B **70** 165114
[10] Blaha P, Schwar K, Madsen G K H, Kvasnicka D and Luitz J 2003 *WIEN2k—An Augmented Plane Wave+ Local Orbitals Program for Calculating Crystal Properties* Techn. Universität Wien, Getreidemarkt 9/156 A-1060 Wien/Austria
[11] Hohenberg P and Kohn W 1964 *Phys. Rev.* B **136** 864
[12] Perdew J P and Wang Y 1986 *Phys. Rev.* B **33** 8800
[13] Kučas S, Kynienė A, Karazija R, Finkelstein L D and Kurmaev E Z 2005 *J. Phys.: Condens. Matter* **17** 7307